Misexpression of *BRE* gene in the developing chick neural tube affects neurulation and somitogenesis

Guang Wang[a,*], Yan Li[a,*], Xiao-Yu Wang[a,*], Manli Chuai[b], John Yeuk-Hon Chan[a], Jian Lei[a], Andrea Münsterberg[c], Kenneth Ka Ho Lee[d], and Xuesong Yang[a]

[a]Department of Histology and Embryology, School of Medicine, Key Laboratory for Regenerative Medicine of the Ministry of Education, Jinan University, Guangzhou 510632, China; [b]Division of Cell and Developmental Biology, University of Dundee, Dundee DD1 5EH, United Kingdom; [c]School of Biological Sciences, University of East Anglia, Norwich NR4 7TJ, United Kingdom; [d]Key Laboratory for Regenerative Medicine of the Ministry of Education, School of Biomedical Sciences, Chinese University of Hong Kong, Shatin, Hong Kong

ABSTRACT The brain and reproductive expression (*BRE*) gene is expressed in numerous adult tissues and especially in the nervous and reproductive systems. However, little is known about *BRE* expression in the developing embryo or about its role in embryonic development. In this study, we used in situ hybridization to reveal the spatiotemporal expression pattern for *BRE* in chick embryo during development. To determine the importance of *BRE* in neurogenesis, we overexpressed *BRE* and also silenced *BRE* expression specifically in the neural tube. We established that overexpressing *BRE* in the neural tube indirectly accelerated Pax7⁺ somite development and directly increased HNK-1⁺ neural crest cell (NCC) migration and TuJ-1⁺ neurite outgrowth. These altered morphogenetic processes were associated with changes in the cell cycle of NCCs and neural tube cells. The inverse effect was obtained when *BRE* expression was silenced in the neural tube. We also determined that BMP4 and Shh expression in the neural tube was affected by misexpression of *BRE*. This provides a possible mechanism for how altering *BRE* expression was able to affect somitogenesis, neurogenesis, and NCC migration. In summary, our results demonstrate that *BRE* plays an important role in regulating neurogenesis and indirectly somite differentiation during early chick embryo development.

Monitoring Editor
Marianne Bronner
California Institute of Technology

Received: Jun 23, 2014
Revised: Dec 2, 2014
Accepted: Dec 23, 2014

INTRODUCTION

The brain and reproductive expression (*BRE*) gene is expressed in a variety of tissues, including the brain, ovary, testis, heart, kidney, and adrenal glands (Li *et al.*, 1995; Miao *et al.*, 2001). The gene is most highly expressed in the nervous and reproductive systems, hence its name. *BRE* is now considered to be an adaptor protein involved in stress response and DNA- damage-repair response by some yet-unknown mechanisms. It is also believed to be a homeostatic or housekeeping protein (Ching *et al.*, 2001), since the gene is capable of modulating the action of hormones and cytokines in stress response, cell survival, and various pathological conditions, such as inflammation, infection, and cancers (Tang *et al.*, 2006). Moreover, *BRE* has also been called "TNFRSF1A modulator" because it can directly bind to tumor necrosis factor receptor 1 (TNFR-1) and modulate TNF signaling (Gu *et al.*, 1998). Recently we reported that *BRE* plays an important role in regulating stem cell differentiation by helping to maintain stemness (Chen *et al.*, 2013). However, the function of *BRE* during embryo development has not yet been investigated. Hence, in this study, we examined how overexpressing and silencing *BRE* expression in the chick embryo neural tube affected development.

The neural tube develops from a bilateral pair of neural plate elevations at the early embryonic stage and subsequently fuses

This article was published online ahead of print in MBoC in Press (http://www.molbiolcell.org/cgi/doi/10.1091/mbc.E14-06-1144) on January 7, 2015.

*These authors contributed equally to this work.

G.W., Y.L., X.-Y.W., and J.L. performed the experiments and collected the data. M.C., J.Y.-H.C., and A. M. analyzed the data. G.W., K.K.H.L., and X. Y. designed the study, analyzed the data, and wrote the manuscript.

The authors declare that no competing interests exist.

Address correspondence to: Xuesong Yang (yang_xuesong@126.com), Kenneth Ka Ho Lee (kaholee@cuhk.edu.hk).

Abbreviations used: *BRE*, brain and reproductive expression; EMT, epithelial to mesenchymal transition; NCC, neural crest cell; NF, neurofilament; PSM, presomitic mesoderm; p-Smad1/5/8, phospho-Smad1/5/8; Shh, sonic hedgehog.

to form a tubular structure extending cranial-caudally. This is a complex morphogenetic process involving cell induction, proliferation, and apoptosis. The neural tube will eventually form the spinal cord and brain at late embryogenesis. During neural tube formation, neural crest cells (NCCs) are formed at the crests of neural plate elevations. These NCCs undergo an epithelial-to-mesenchymal transition (EMT) as the neural tube closes and migrate throughout the embryo, where they differentiate into a host of different cell types (Huang and Saint-Jeannet, 2004; Bronner, 2012; Bronner and LeDouarin, 2013). These dynamic processes associated with NCC emergence, migration, and development could be regarded as a continual process of cellular differentiation, that is, the transition of premigratory NCCs in the dorsal neural tube into migratory NCCs and then their migration beneath the neuroepithelium or between the somites and neural tube. Like NCCs, somites are also transient embryonic structures. They are derived from the paraxial mesoderm and take the form of a paired spherical body localized on each side of neural tube (Christ *et al.*, 1992; Noden *et al.*, 1999). The somites appear cranially and extend caudally to the tail end of the chick embryo. They differentiate to form the dermatome, myotome, and sclerotome, which in turn become the dermis, skeletal muscles, and cartilage and connective tissues (Christ and Ordahl, 1995; Kageyama *et al.*, 2012; Eckalbar *et al.*, 2013).

It is now well established that the neural tube, somites, and notochord closely interact with each other to regulate normal development. During somitogenesis, inhibitory and stimulatory signals generated from the surrounding tissues (such as the notochord, floor plate, neural tube, dorsal ectoderm, and lateral mesoderm) regulate somite morphogenesis and differentiation (Lee *et al.*, 1995; Francetic and Li, 2011). Signals from the dorsal neural tube affect the development of the somite-derived dermomyotome and myotome (Munsterberg *et al.*, 1995; Marcelle *et al.*, 1997; Sela-Donenfeld and Kalcheim, 2002; Serralbo and Marcelle, 2014), and it has been reported that migrating NCCs affect somite differentiation (Rios *et al.*, 2011; Serralbo and Marcelle, 2014). Reciprocally, the medial lip of the dermomyotome inhibits the transcription of noggin in the neural tube, which relieves repression from bone morphogenic protein (BMP) signaling and stimulates the emigration of NCCs. The migration of NCCs to the ventral and dorsal sides of the somites is involved in regulating somitic myogenesis (Kalcheim, 2011). The notochord and floor plate generate sonic hedgehog (Shh) protein, an important morphogen, which controls many important morphogenetic events in the embryo, including somite development. Shh can transiently control somite formation (Resende *et al.*, 2010) and promote somitic chondrogenesis (Murtaugh *et al.*, 1999) and myogenesis by inducing Myf5 expression directly and MyoD indirectly (Chiang *et al.*, 1996). Inversely, factors produced in a rostrocaudal pattern by the somites could confine the movement of spinal motor axons and NCCs to the rostral half of the somitic sclerotome (Koblar *et al.*, 2000).

In this study, we first defined the spatiotemporal expression pattern of *BRE* during early chick embryo development. We then examined the effects of overexpressing and silencing *BRE* in the neural tube to elucidate the importance of this gene in NCC migration, somite development, neurite outgrowth, and cell cycle.

RESULTS

BRE is expressed in the developing neural tube and somites

In situ hybridization was performed on chick embryos to establish where *BRE* was spatiotemporally expressed at the primitive streak (HH4) stage to the heart formation (HH12) stage (Figure 1). In stage HH4 chick embryos, the primitive streak has elongated to attain its overall length. The neural plate, which will give rise to the neural tube, has also fully formed. *BRE* is found mainly expressed in the neural plate at this stage (Figure 1A). In transverse sections, *BRE* could be seen strongly expressed in the epiblast cells around the primitive streak (neural plate; Figure 1A, 1–4). *BRE* was also expressed in the mesoderm layer directly beneath the epiblast, although weaker when compared with the neural plate. In stage HH8–10 embryos, *BRE* was expressed mainly in closing (Figures 1B, 1 and 2) and closed (Figure 1C1) rostral neural tube (derived from the neural plate), which indicates continuous expression for *BRE* in the neural tissues. Cranial NCCs also expressed *BRE* (Figure 1C2). This suggests that *BRE* might be involved in the migration of NCCs. *BRE* was also expressed in developing somites, although relatively weakly (Figure 1C3). In stage HH12 chick embryos, *BRE* was expressed in the neural tube (Figure 1D) but not as intensely as in earlier-stage embryos (Figure 1D1). In contrast, *BRE* expression dramatically increased in head mesenchymal tissues and trunk somites (Figure 1D, 1–3), implying that *BRE* might also be involved in somite development and differentiation.

Overexpressing *BRE* in the neural tube accelerates somitogenesis

We have validated that *BRE* is expressed in the neural tube, using in situ hybridization. Hence we asked whether neural tube development would be affected when we misexpressed *BRE*. We injected and electroporated constructs containing the full-length *BRE* (*BRE*-wt) or small interfering RNA (*BRE*-siRNA) into the neural tube to overexpress or silence *BRE* expression, respectively (Figure 1E). Electroporation was performed so that one side of the neural tube was transfected with the construct and the contralateral half was untransfected and served as the control. In situ hybridization was performed to confirm that *BRE* expression has been ipsilaterally silenced using our *BRE*-siRNA (Figure 1F) or ipsilaterally overexpressed after transfection with our *BRE*-wt construct (Figure 1, G and G1) in the neural tube. Using semiquantitative real-time (RT)-PCR and quantitative PCR, we confirmed that *BRE* expression could be significantly up-regulated after *BRE*-wt transfection (Figure 1H and Supplemental Figure S1A; control–green fluorescent protein [GFP], 0.98 ± 0.04, and *BRE*-wt, 1.28 ± 0.09; $p < 0.05$, $N = 8$) or down-regulated after *BRE*-siRNA transfection (Figure 1H, $N = 3$).

Then immunofluorescence staining was performed for Pax7, which labels the dorsal side of neural tube, somites, and dermomyotome derivatives (Figure 2, A–G; Otto *et al.*, 2006; Galli *et al.*, 2008). We determined that the neural tube unilaterally cotransfected with control-siRNA plus GFP constructs has no effect on the $Pax7^+$ somites and neural tube (Figure 2, A–B2, I, and J). Surprisingly, we found $Pax7^+$ somites were larger on the side of the neural tube that overexpressed *BRE* than the control side ($N = 8/10$; Figure 2, C and J). In corresponding transverse sections, the affected somites have differentiated to form a wide strip of $Pax7^+$ dermomyotome, whereas on the control side, the dermomyotome was smaller and less differentiated (Figure 2, D1, D2, and I). At more caudal levels, where the somites are less mature, the larger somites on the *BRE*-overexpressed side of the neural tube were still clearly evident (Figure 2, E1, E2, and I; transfection-side somite area vs. control-side somite area: control-GFP, 0.98 ± 0.09, and *BRE*-wt, 1.57 ± 0.15; $p < 0.001$). Next we silenced *BRE* expression in half of the neural tube; this inhibited somite development ($N = 7/10$; Figure 2, F and J). In corresponding transverse sections, we found that the length of the $Pax7^+$ dermomyotome on the *BRE*-silenced side of the neural tube (left) was smaller than on the contralateral control side (Figure 2, G1 and G2), suggesting that reduced *BRE* expression in the neural tube indirectly interfered with somite

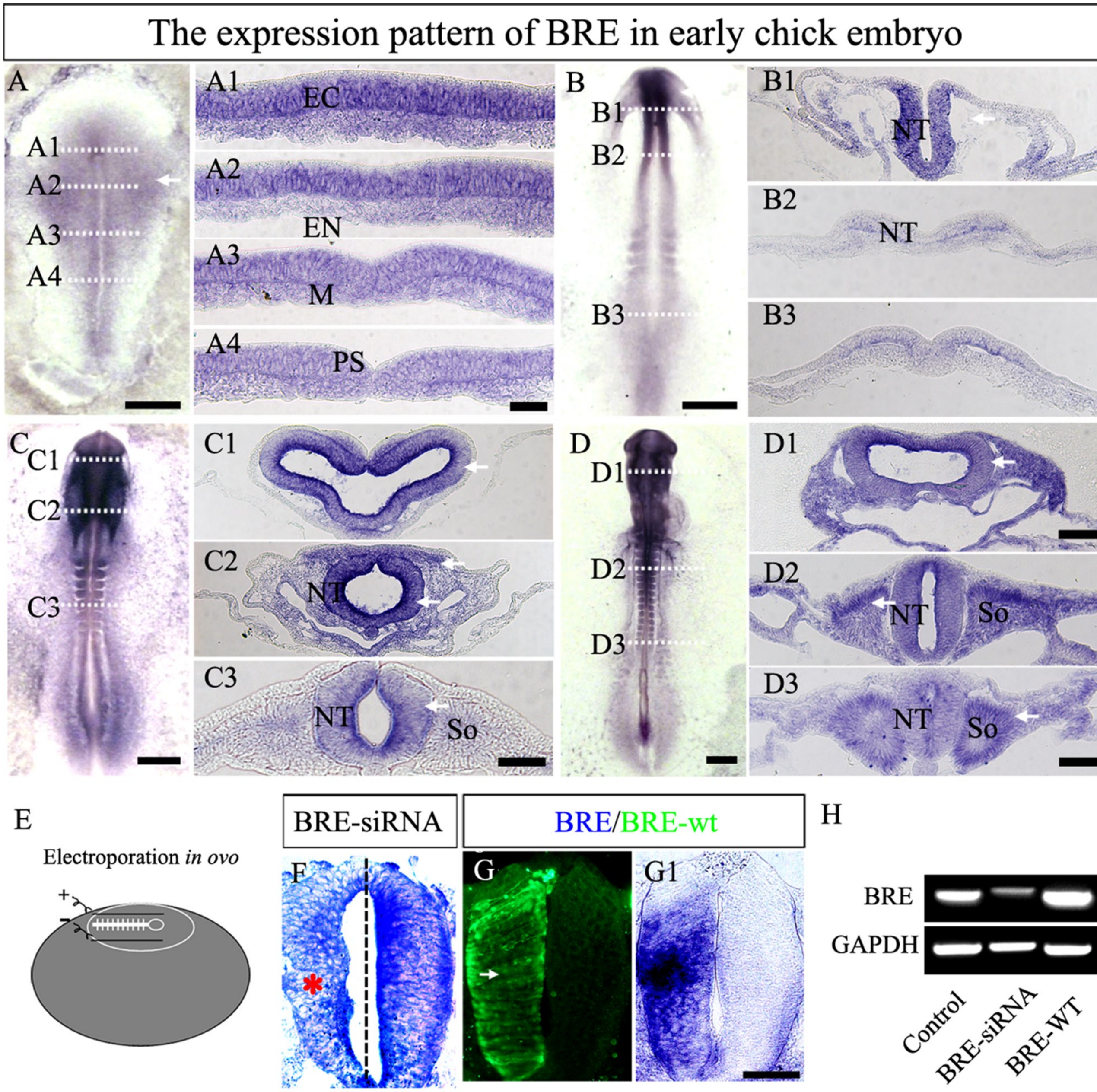

FIGURE 1: Expression pattern of *BRE* in the early chick embryo. Whole-mount in situ hybridization for *BRE* expression was performed on stage HH4, 8, 10, and 12 embryos. (A) In HH4 chick embryos, *BRE* was expressed mainly in the neural plate. The embryo was transversely sectioned along the rostral–caudal axis (A, A1–A4) as indicated by the dotted white lines. (A1–A4) *BRE* was mainly expressed in the ectoderm (EC) of the neural plate region and weakly in the lateral mesoderm (M) along the embryonic rostral–caudal axis. (B) In HH8 chick embryos, *BRE* was mainly expressed in the head folds, closing neural folds, and regressing primitive streak. (B1–B3) Transverse sections of B, showing *BRE* expressed in the closing neural folds and the neuroepithelial site adjacent to the underlying mesoderm layer. (C) *BRE* was mainly expressed in the forebrain, midbrain, hindbrain, and trunk neural tube of HH10 embryos. (C1–C3) Transverse sections of C showing that *BRE* was expressed in the cranial neural tube and in NCCs located at the heart tube and trunk neural tube levels. (D) In HH12 chick embryo, *BRE* was dispersedly expressed in the neural tube and more intensely expressed in mesodermal structures, such as somites. (D1–D3) Transverse sections of D showing that *BRE* was mainly expressed in somites, brain, and trunk neural tube (although the last two tissues more weakly compared with younger embryos). (E) Schematic drawing depicting how our gene constructs were transfected into the neural tube of chick embryos in ovo. (F) In situ hybridization showing that the endogenous *BRE* was silenced after *BRE*-siRNA transfection (left). (G, G1) In situ hybridization showing that *BRE* expression (white arrows) was increased after unilateral cotransfection of the neural tube with *BRE*-wt and GFP (left). (H) Semiquantitative RT-PCR analysis confirmed that *BRE* expression was increased after transfection with *BRE*-wt construct and decreased after transfection with *BRE*-siRNA ($N = 3$). Scale bars, 500 μm (A–D), 20 μm (A1–A4), 50 μm (B1–B3, C1, C2, D2, D3, F, G1), 25 μm (C3), 100 μm (D1). EC, ectoderm; EN, endoderm; M, endoderm; NT, neural tube; PS, primitive streak; So, somite.

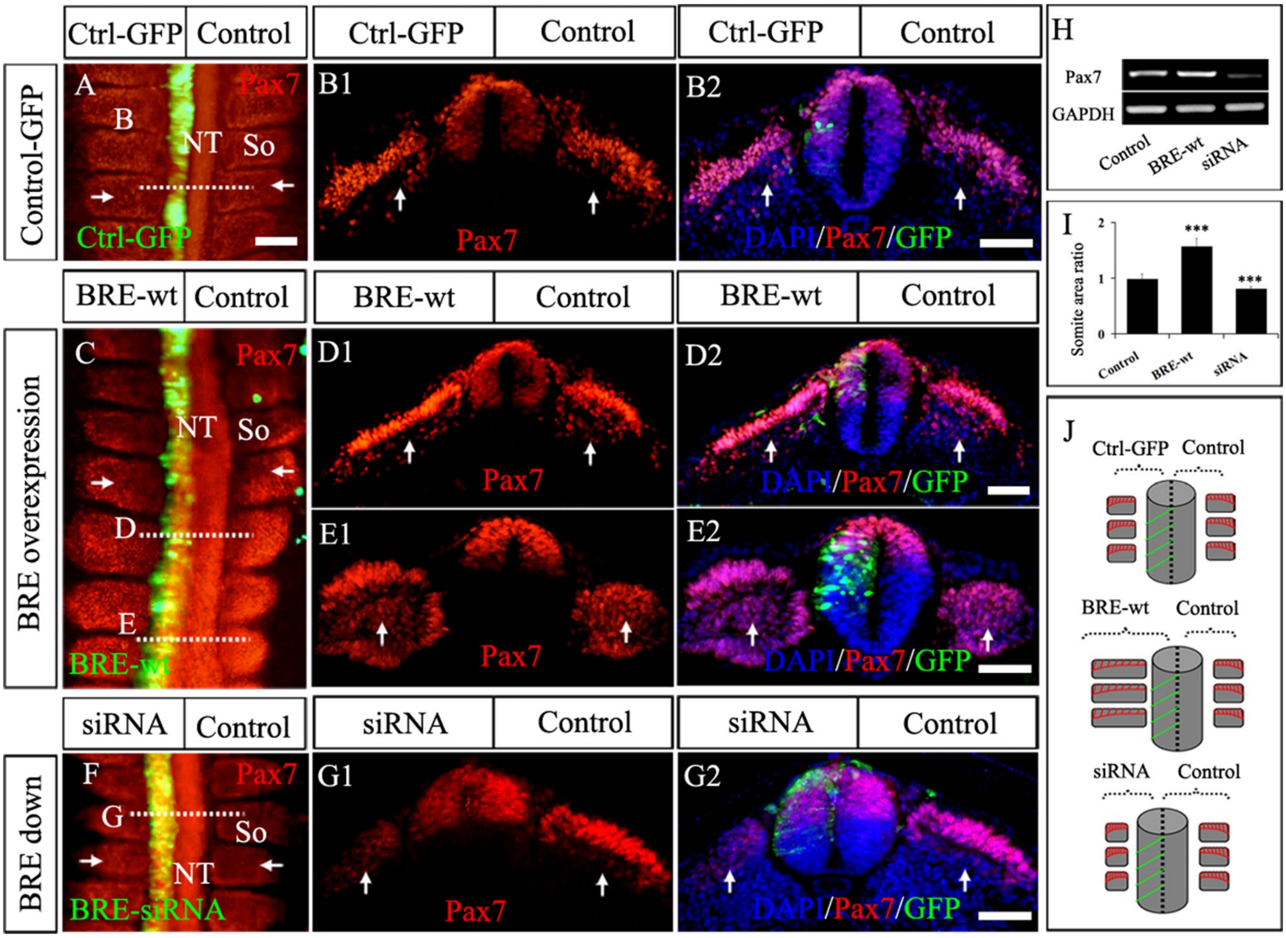

FIGURE 2: Somite differentiation is affected by misexpressing *BRE* in neural tube. (A) Representative whole-mount embryo showing the neural tube unilaterally cotransfected with control-siRNA plus GFP constructs, cultured, and then immunofluorescently stained for Pax7 expression. The somites of the transfection side (white arrows) are similar to the somites on the contralateral side of the untransfected neural tube. *N* = 10/10 embryos. (B1, B2) Transverse section indicated by white dotted line B in A. (B1) Pax7-labeled somites in the transfection side of neural tube are similar to those on the contralateral control side. (B2) Merge of B1with GFP and DAPI staining. (C) Representative whole-mount embryo showing the neural tube unilaterally cotransfected with *BRE*-wt plus GFP constructs, cultured, and then immunofluorescently stained for Pax7 expression. The somites adjacent to left side of the neural tube, which overexpresses *BRE*, are grossly larger than the somites on the contralateral side of the untransfected neural tube. Somite differentiation is indicated by Pax7 expression (white arrows) and shows that *BRE* overexpression in the neural tube indirectly enhanced somite differentiation (wider somite formed). *N* = 8/10 embryos. (D1, D2) Transverse section indicated by white dotted line D in C. (D1) Pax7 marker in the dorsal neural tube and somites. The Pax7-labeled somites in the *BRE* overexpressed side of neural tube differentiated faster and more extensively (dermomyotome formation indicated by white arrows) than on the contralateral control side. (D2) Merge image of D1 with GFP and DAPI staining. (E1, E2) Transverse section indicated by white dotted line E in C. (E1) Pax7-labeled dorsal neural tube and somites. The somites in E1 are less mature than in D1, but, as in D1, the somites on the *BRE* overexpressed side of neural tube are significantly bigger (white arrows) than on the contralateral control side. (E2) Merge image of E2 with GFP and DAPI staining. (F) Representative whole-mount embryo showing the neural tube unilaterally cotransfected with *BRE*-siRNA plus GFP constructs, cultured, and then immunofluorescently stained for Pax7 expression. The somites opposing the *BRE*-silenced side of the neural tube are significantly smaller (white arrows) than the somites on the contralateral side of the untransfected neural tube. *N* = 7/10 embryos. (G1, G2) Transverse section indicated by white dotted line G in F. (G1) Pax7-labeled somites on the *BRE*-silenced side of neural tube are smaller and differentiation retarded (shorter dermomyotome formed) compared to those on the contralateral control side. (G2) Merge of G1with GFP and DAPI staining. (H) Semiquantitative RT-PCR analysis of the neural tube transfected with control-GFP, *BRE*-wt, or *BRE*-siRNA constructs. *BRE* overexpression enhanced Pax7 expression, whereas silencing *BRE* decreased Pax7 expression compared with the control. *N* = 3. (I) Bar chart of the somite area ratio (transfection side vs. control side from the sections) in control, *BRE*-wt, and *BRE*-siRNA– transfected embryos (*N* = 10). (J) Schematic illustrations showing that the neural tube unilaterally cotransfected with control-siRNA plus GFP constructs has no effect on the differentiation of somites. However, *BRE* overexpression in the neural tube indirectly accelerates somite differentiation (middle), whereas silencing *BRE* retarded somite differentiation (bottom). Scale bar, 100 μm (A, C, F), 20 μm (B1, B2, D1–D3, E1, E2, G1, G2). Ctrl-GFP, control-GFP; NT, neural tube; So, somite.

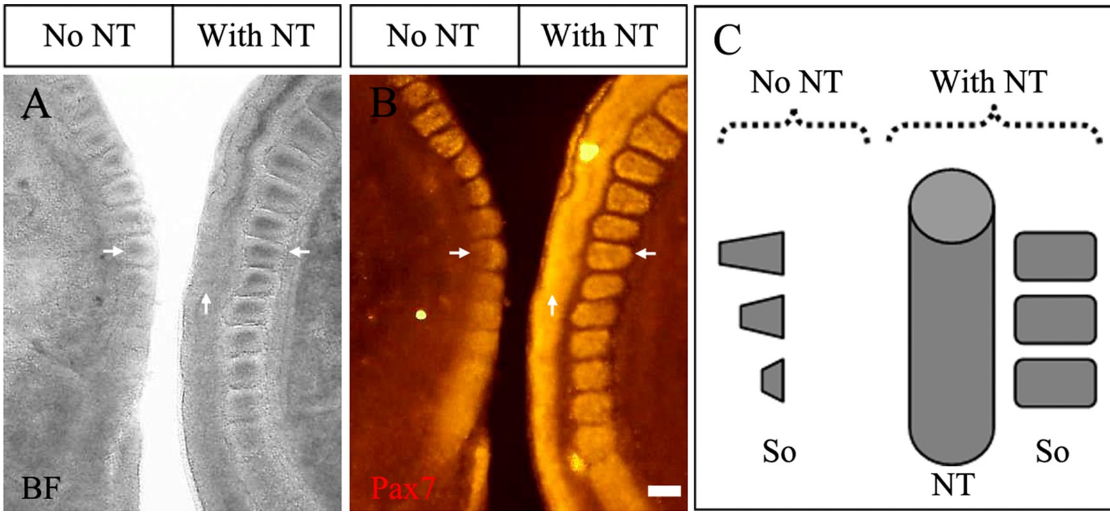

FIGURE 3: Presence of the neural tube is required for normal somite development. Somite development was compared in the presence or absence of neural tube in explant culture. A HH10 chick embryo was sliced into two parts along the rostral–caudal axis and then cultured 24 h. (A) The left explant contained somites that developed in the absence of neural tube, whereas for the right explant, the somites developed in the presence of neural tube. (B) Immunofluorescence staining for Pax7 was performed on explant cultures in A. In both bright-field and Pax7 IHC images, the somites developed normally in the presence of neural tube. In contrast, in the absence of the neural tube, somite development was retarded and abnormal, illustrating the importance of the neural tube in somitogenesis (C). Scale bar, 100 μm. NT, neural tube; So, somite.

development and differentiation (Figure 2I; transfection-side somite area vs. control-side somite area: *BRE*-siRNA, 0.81 ± 0.04; $p < 0.001$). Furthermore, the level of Pax7 expression was confirmed by semiquantitative RT-PCR and quantitative PCR analysis after electroporation with *BRE*-wt and *BRE*-siRNA (Figure 2H; control-GFP, 0.98 ± 0.04; *BRE*-wt, 1.39 ± 0.16; $p < 0.05$, $N = 7$; Supplemental Figure S1B). The quantitative PCR results showed that Pax3, another gene involved in somite differentiation, was also increased after *BRE* overexpression in the neural tube compared with control samples (control-GFP, 0.91 ± 0.14, *BRE*-wt, 2.63 ± 0.63; $p < 0.05$, $N = 7$; Supplemental Figure S1C).

Neural tube is required for proper somitogenesis and differentiation

Developmentally, there is a very close relationship between the somites and neural tube. It has been proposed that inhibitory cross-talk between the paraxial mesoderm and neural primordium controls the timing of neural crest delamination to match the development of a suitable mesodermal substrate for subsequent NCC migration (Sela-Donenfeld and Kalcheim, 2000). Our foregoing data show that somites developed asymmetrically when the opposing side of the neural tube overexpressed *BRE*. To confirm directly that there is cross-talk between the somite and neural tube, we cultured explants composed of somite and presomitic mesoderm (PSM) devoid of the neural tube or explants composed of somite and PSM plus neural tube (Figure 3) in vitro at 37°C for 48 h. Immunofluorescence staining for Pax7 clearly demonstrated that somites develop and differentiate much faster in the presence of the neural tube than in its absence (Figure 3B). This confirms that somite development and differentiation are dependent on signals emitted from ipsilateral neural tube.

BRE modulates NCC migration and neurite outgrowth

Normally, NCCs delaminate from the dorsal neural tube of the trunk, with one population of NCCs migrating through the rostral half of adjacent differentiating somites. This raises the possibility that the larger somites formed on the *BRE*-transfected neural tube side might be a consequence of NCC invasion. To address this question, we performed immunofluorescence staining against HNK-1 (a maker for migrating NCCs) after ipsilateral *BRE* overexpression or silencing on one side of the neural tube (Figure 4). In control embryos, we ipsilaterally transfected the neural tube with a GFP-only construct and stained the embryos with HNK-1 antibody to demonstrate the normal extent of NCC migration (Figure 4, A–D, $N = 6$ embryos). The results show that our electroporation technique did not physically damage the neural tube to prevent NCC migration. When we ipsilaterally overexpressed *BRE* in the neural tube, we found that NCC migration was significantly increased on the *BRE*-transfected side in 93% of embryos as compared with the contralateral control side (Figure 4, E–H and M; $N = 14$ embryos). Conversely, NCC migration was reduced when *BRE* expression was ipsilaterally silenced in the neural tube (Figure 4, I–L and M, $N = 8$ embryos). We then calculated the area occupied by HNK-1$^+$ cells in the *BRE*-manipulated neural tube side versus the control side. The ratio GFP/control was 0.97 ± 0.03 ($N = 8$ sections; Figure 4N), *BRE*-wt/control was significantly increased at 2.01 ± 0.21 ($N = 8$ sections, $p < 0.01$; Figure 4N), and *BRE*-siRNA/control was significantly reduced at 0.42 ± 0.04 ($N = 8$ sections, $p < 0.001$; Figure 4N). Together the results suggest that overexpression of *BRE* enhances the migration of NCCs (Figure 4O), which then invade the differentiating somites, making them appear larger than normal. Besides HNK-1, we examined other neural crest–specifier genes (Snail2, MSX1, FoxD3, and Sox9) by quantitative PCR analysis (Supplemental Figure S1, D–G). We found that overexpressing *BRE* did not affect Snail2 and MSX1 but increased FoxD3 and reduced Sox9 expression. In situ hybridization confirmed that *BRE* hardly affects Snail2 expression ($N = 3$ embryos in each group; Supplemental Figure S2).

Besides NCC delamination, neurites also grow out from the developing neural tube. Hence we want to establish whether altering *BRE* expression affects this process. Neurofilament (NF) antibody

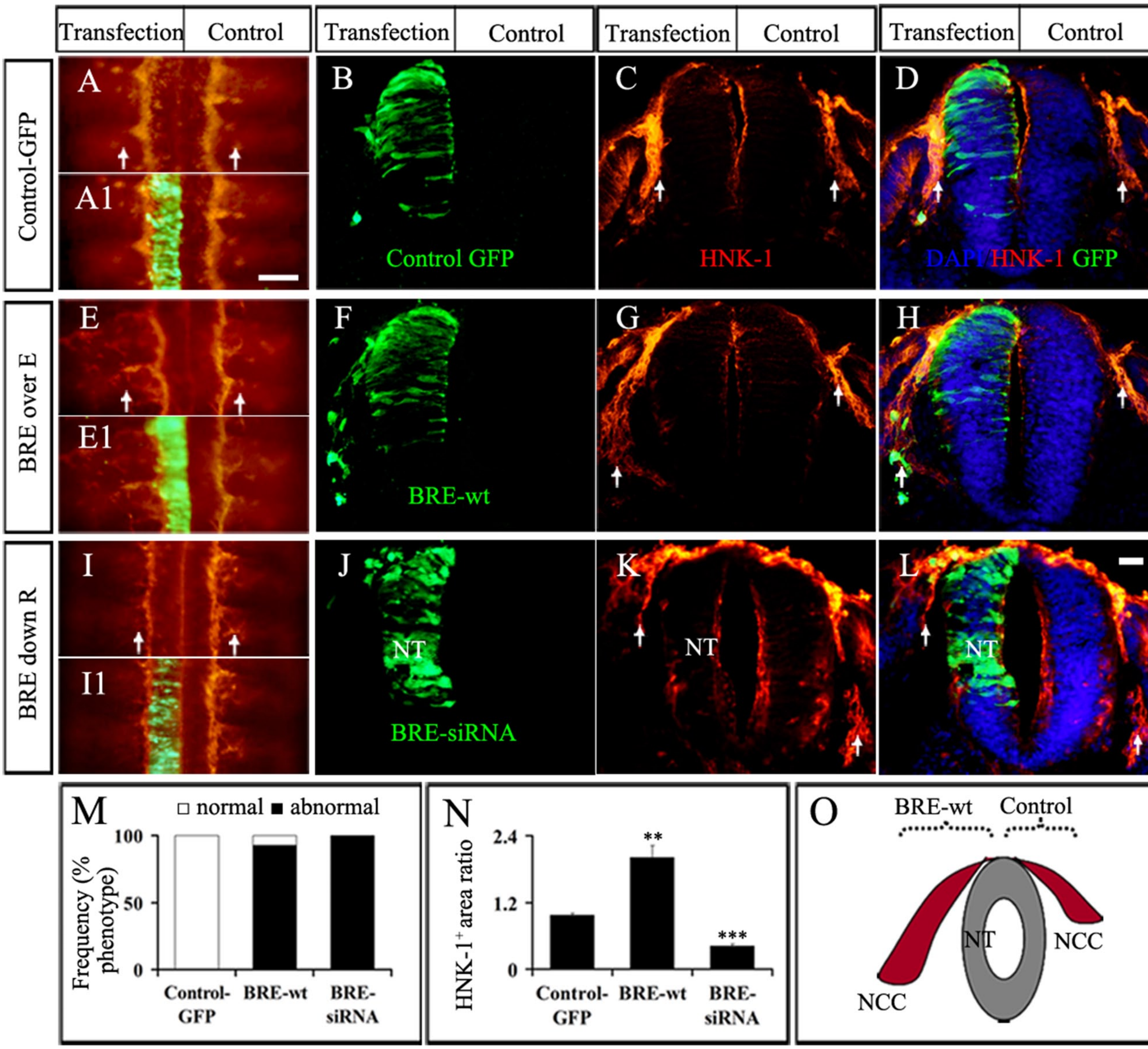

FIGURE 4: Effects of overexpressing and silencing *BRE* in the neural tube on NCC migration. (A-D) The neural tube was unilaterally cotransfected with control-siRNA plus GFP constructs. (A) Immunofluorescence staining for HNK-1 labels the migrating NCCs on both sides of the neural tube (white arrows). (A1) Merge image of HNK-1 and GFP. (B) Left side of the neural tube expressing GFP in section. (C) Immunofluorescence staining for HNK-1 labels the migrating NCCs on both sides of the neural tube (white arrows) in section. (D) Merge image of A and B stained with DAPI. (E–H) The neural tube was unilaterally transfected with *BRE*-wt. (E) HNK-1^+ NCCs migrating more extensively on the neural tube side overexpressing *BRE* than on the nontransfected side (white arrows). (E1) Merge image of HNK-1 and GFP. (F) Left side of the neural tube overexpressing *BRE*. (G, H) HNK-1^+ NCCs migrating more extensively on the neural tube side overexpressing *BRE* than on the nontransfected side (white arrows) in section. (I–L) The neural tube was unilaterally cotransfected with *BRE*-siRNA and GFP constructs. (I) HNK-1^+ NCC migration was reduced on the silenced *BRE* neural tube compared with NCC migration on the nontransfected side (white arrows). (I1) Merge image of HNK-1 and GFP. (J) Left side of the neural tube silenced by *BRE*-siRNA and expressing GFP. (K, L) HNK-1^+ NCC migration was reduced on the silenced *BRE* neural tube compared with NCC migration on the nontransfected side (white arrows) in section. (M) Bar chart showing abnormal NCC migration (black) after *BRE* overexpression and silencing (*BRE*-wt, $N = 14$ embryos; *BRE*-siRNA, $N = 8$ embryos). (N) Bar chart showing the relative area in the embryo invaded by HNK-1^+ NCCs in control, *BRE*-wt, and *BRE*-siRNA–transfected embryos ($N = 8$ sections/embryo, $^{**}p < 0.01$, $^{***}p < 0.001$). (O) Schematic illustration showing that *BRE* promotes NCC migration. Error bars, SE. Scale bar, 100 μm (A, A1, E, E1, I, I1), 20 μm (B–D, F–H, and J–L). NT, neural tube.

was used to label intermediate filaments within neurites, which protrude from anterior horns of the spinal cord (Supplemental Figure S3, D1 and D2). Control-GFP transfection confirmed that the electroporation did not harm the neural tube and was able to produce neurite outgrowths (Figure 5, A, A1, and D; $N = 6$ embryos). We found that ipsilaterally overexpressing *BRE* resulted in an earlier appearance of NF^+ neurite outgrowth from the anterior horn in 92% of embryos as compared with the contralateral control side (Figure 5, B, B1, and E; $N = 13$ embryos). In contrast, silencing *BRE* expression resulted in a delay in the appearance of NF^+ neurites in 86% of the

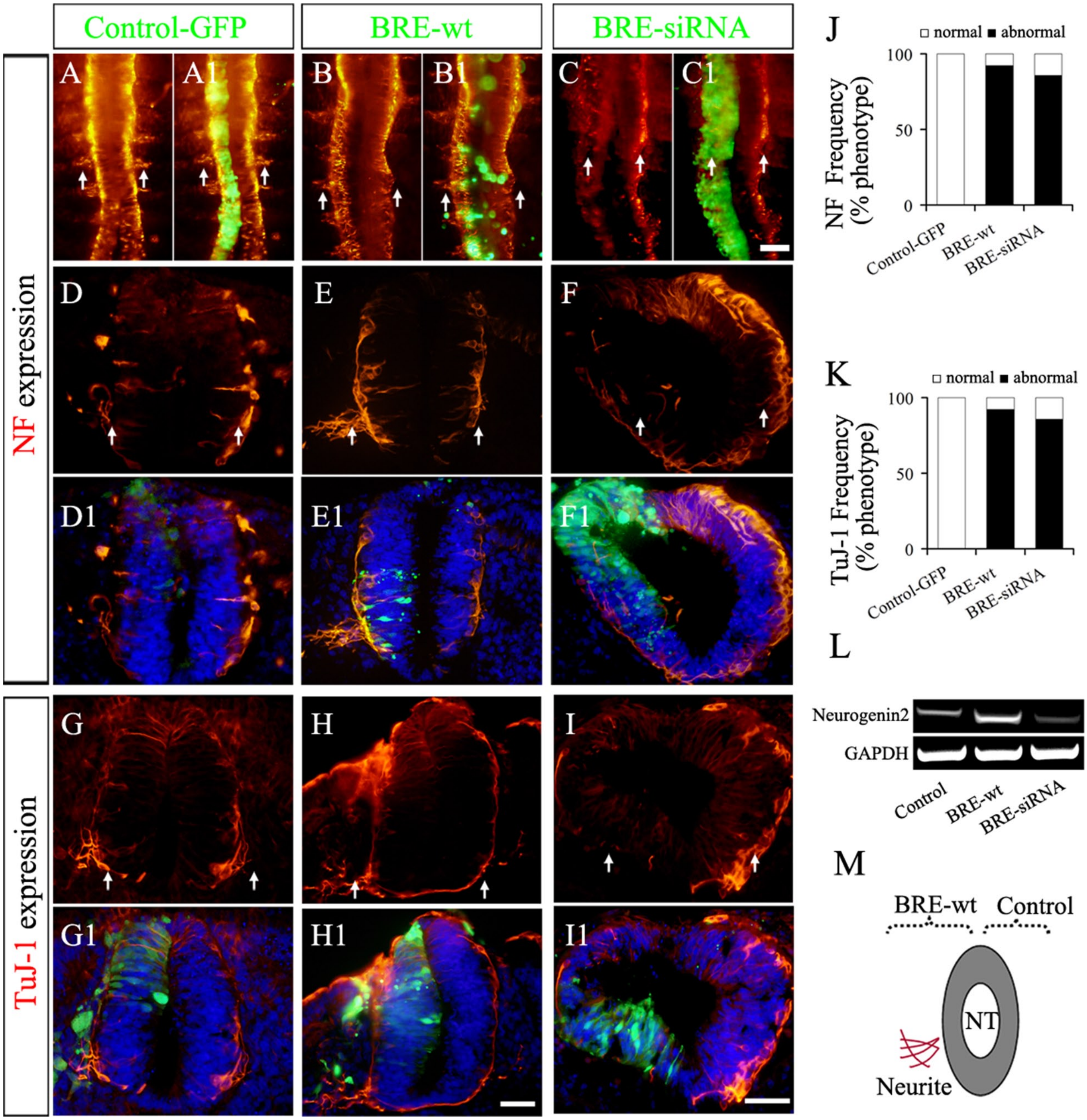

FIGURE 5: *BRE* affects the initiation of motor neuron outgrowth from the neural tube anterior horns. *BRE* was overexpressed or silenced on the left side of HH10 neural tube. The embryos were cultured, and the motor neurons started to develop and were stained with NF (A–F) and TuJ-1 (G–I) antibodies. (A–C) Whole-mount immunohistochemistry against NF to label the neurites. (A1–C1) Merge images of GFP and NF staining. (D–F) Transverse sections. (A, A1, D) Left side of the neural tube transfected with control-GFP constructs, showing that NF expression is symmetrical on both sides of the neural tube. (B, B1, E) Left side of the neural tube cotransfected with *BRE*-wt and GFP constructs, showing more NF$^+$ cells on the *BRE*-overexpressed side than on the untransfected side, as indicated by white arrows. (C, C1, F) Left side of the neural tube cotransfected with *BRE*-siRNA and GFP constructs, showing fewer NF$^+$ cells on the *BRE*-silenced side than on the untransfected side, as indicated by the white arrows. (G, G1) Left side of the neural tube transfected with control-GFP construct, showing that TuJ-1$^+$ cells are symmetrically distributed on both sides of the neural tube (white arrows). (H, H1) Left side of the neural tube cotransfected with *BRE*-wt and GFP constructs, showing that there are more TuJ-1$^+$ cells on the side overexpressing *BRE* than on the nontransfected side (white arrows). (I, I1) Left side of the neural tube cotransfected with *BRE*-siRNA and GFP constructs. There are fewer TuJ-1$^+$ cells on the *BRE*-silenced side than on the nontransfected side. (J) Bar chart showing that NF$^+$ neurite outgrowth is affected (black) by *BRE* misexpression (control-GFP, 6 embryos; *BRE*-wt, 7 embryos; *BRE*-siRNA, 8 embryos). (K) Bar chart showing that TuJ-1$^+$ neurite outgrowth is affected (black) by *BRE* misexpression (control-GFP, 6 embryos; *BRE*-wt, 13 embryos; *BRE*-siRNA, 7 embryos). (L) Semiquantitative RT-PCR analysis showing that *BRE* overexpression in the neural tubes increased Neurogenin2 expression, whereas silencing *BRE* reduced Neurogenin2 expression ($N = 3$). (M) Schematic drawing illustrating that *BRE* promotes motor neurite outgrowth from anterior horns. Scale bar, 100 μm (A–C), 50 μm (D, E1, F, F1, G, H1, I, I1). NT, neural tube.

embryos examined; the phenotype can be easily observed on the rostral side (Figure 5, C, C1, and F; $N = 7$ embryos). We also used the TuJ-1 neuron marker to confirm our observation. TuJ-1 identifies neuron-specific class III β-tubulin. The neural tube was unilaterally transfected with control-GFP (Figure 5, G, G1, and K; $N = 6$ embryos), *BRE*-wt, or *BRE*-siRNA constructs. The results were consistent with the NF-staining patterns, where TuJ-1^+ neurites grew out earlier from the side of the neural tube that overexpressed *BRE* than the control side in 86% of the embryos (Figure 5, H, H1, and K; $N = 7$ embryos). Conversely, silencing *BRE* expression delayed the outgrowth of the TuJ-1^+ neurites in 88% of the embryos examined (Figure 5, I, I1, and K; $N = 8$ embryos). In addition, we used semiquantitative PCR to detect Neurogenin2, a basic helix-loop-helix transcription factor that functions in neuronal differentiation (Simmons *et al.*, 2001). Neurogenin2 was up-regulated after *BRE*-wt transfection and down-regulated after *BRE*-siRNA transfection (Figure 5L). In sum, altered levels of *BRE* expression can affect neurite outgrowth from the neural tube (Figure 5M).

BRE modulates cell cycle progression and survival in the developing neural tube

We investigated whether there was any association between *BRE* expression and cell cycle, which would help explain why NCC migration and neurite outgrowth were abnormal. We established that 68.01 ± 1.60% of *BRE*-overexpressing (GFP^+) cells were bromodeoxyuridine positive ($BrdU^+$), whereas 49.03 ± 1.56% of control GFP^+ were $BrdU^+$. This implies that that *BRE* overexpression significantly accelerated cells into S phase compared with control cells in the neural tube ($p < 0.001$; Figure 6, A–A2, B–B2, and J). In contrast, there were significantly fewer *BRE*-silenced (GFP^+) cells that were $BrdU^+$ cells (43.06 ± 1.11%) than the control ($p < 0.05$; Figure 6, C–C2 and J). In the *BRE*-overexpressed group, we also found GFP^+ and $BrdU^+$ colocalization in NCCs, as indicated by arrows (Figure 6, B–B2). In addition, we found that $BrdU^+$ cells in the *BRE*-wt–transfected side were greater than on the contralateral control side in somites (control-GFP, 0.96 ± 0.03, $N = 6$; *BRE*-wt, 1.72 ± 0.06, $N = 12$; ***$p < 0.001$; Supplemental Figure S4, A–D and G). Conversely, the $BrdU^+$ cells in the *BRE*-siRNA–transfected side of somites were fewer (*BRE*-siRNA, 0.70 ± 0.02, $N = 12$; ***$p < 0.01$; Supplemental Figure S4, A–B and E–G). These results imply that *BRE* is also involved in neural tube, NCC, and somite development by modulating the cell cycle.

We next examined the effects of altered *BRE* expression on cyclin D1 expression, since the latter is indispensable for G1/S cell cycle transition. Using in situ hybridization, we showed that cyclin D1 expression was little affected in the control group (Figure 6, D, D1, and K; $N = 6$). When *BRE* was overexpressed, cyclin D1 expression was correspondingly increased in the *BRE*-wt–transfected side of the neural tube in 60% of the embryos (Figure 6, E, E1, and K; $N = 5$). Conversely, silencing of *BRE* expression reduced cyclin D1 expression in 100% of the embryos examined (Figure 6, F, F1, and K; $N = 6$). Furthermore, the extent of cyclin D1 expression in the neural tube was validated by semiquantitative RT-PCR analysis after electroporation with *BRE*-wt or *BRE*-siRNA (Figure 6L). These data suggest that *BRE* promotes G1-S transition. Aberrant cell cycle reactivation in postmitotic neurons could lead to apoptosis (Becker and Bonni, 2005), and cyclin D1 is essential for regulating neuronal cell death (Kranenburg *et al.*, 1996). Hence we examined whether cell survival was altered after *BRE*-wt and *BRE*-siRNA transfection. Terminal deoxynucleotidyl transferase dUTP nick end labeling (TUNEL) assay revealed that there was no significant difference in the ratio (transfection side vs. control side) of $TUNEL^+$ between the control-GFP group and the *BRE*-wt group (Figure 6, G, H, and M; control, 1.15 ± 0.07, and *BRE*-wt, 1.24 ± 0.09; $p > 0.05$). However, there are more apoptotic cells present in the *BRE*-silenced side of the neural tube than the control side (Figure 6, I and M; *BRE*-siRNA, 1.93 ± 0.15; $p < 0.001$). We also found that p53 and BRCA1, which can regulate the cell cycle (Agarwal *et al.*, 1995; Deng, 2006), were significantly decreased (Supplemental Figure S1H) or increased (Supplemental Figure S1I), respectively, after overexpressed *BRE*.

BRE regulates gene expression pattern along the dorsoventral neural tube

BMP4 and Shh are two important genes expressed in the dorsoventral neural tube, and they also play crucial roles in somite differentiation (Murtaugh *et al.*, 1999; Anderson *et al.*, 2009; Resende *et al.*, 2010; Kalcheim, 2011; Van Ho *et al.*, 2011) and neuron differentiation in the ventral neural tube (Wilson and Maden, 2005; Ribes and Briscoe, 2009). Hence we investigated whether influence of *BRE* on the neural tube, NCC, and somite development was mediated by BMP4 and Shh signaling. We performed in situ hybridization to examine BMP4 and Shh expression after *BRE* overexpression and silencing in the neural tube. We found that ipsilateral transfection of the neural tube with our GFP construct (control) did not affect BMP4 expression in the dorsal neural tube or Shh expression in notochord and ventral neural tube. Both genes were expressed symmetrically (Figure 7, A, A1, B, and B1, $N = 3/3$). After *BRE* overexpression, we found BMP4 expression correspondingly up-regulated at the affected ipsilateral neural tube side (Figure 7, C and C1; $N = 3/4$). When *BRE* expression was silenced, we determined that BMP4 expression was reduced in the neural tube (Figure 7, E and E1; $N = 3/5$). In contrast, Shh expression in the ventral neural tube was inhibited after *BRE* overexpression (Figure 7, D and D1; $N = 4/6$), and enhanced after *BRE* silencing (Figure 7, F and F1; $N = 4/6$). We validated these observations by semiquantitative RT-PCR analysis (Figure 7G). The results imply that *BRE* promotes BMP4 expression in the dorsal neural tube and inhibits Shh expression in the ventral neural tube (Figure 7H). BMP and Wnt family members are known to antagonize Shh expression and play an important role in the patterning of the dorsal axis (Patten and Placzek, 2002; Ulloa and Marti, 2010). Thus we also detected whether Wnt signaling was affected after *BRE* transfection. The results showed that *BRE* overexpression could up-regulate β-catenin, whereas *BRE* silencing could down-regulate β-catenin (Supplemental Figure S5).

Overexpressing *BRE* in the neural tube activated BMP signaling

We examined the expression of p-Smad1/5/8 after we overexpressed *BRE*. In control embryos, we ipsilaterally transfected the neural tube with a GFP-only construct and stained the embryos with p-Smad1/5/8 antibody to demonstrate that our electroporation technique did not cause any nonspecific changes ($N = 3/3$; Figure 8, A and A1). When we ipsilaterally overexpressed *BRE* in the neural tube, we found that p-Smad1/5/8 was significantly increased on the *BRE* transfected–side compared with the contralateral control side ($N = 4/4$; Figure 8, B and B1). Next we used in vitro experiments and added LDN-193189, which can inhibit the p-Smad1/5/8 (Yu *et al.*, 2008), to rescue *BRE* effects by BMP modulation. The neural tubes were cotransfected with control-GFP plus control-siRNA or *BRE*-wt or control-GFP plus *BRE*-siRNA and then explanted into culture dishes at 37°C with 5% CO_2 for 48 h. These cultured neural tube explants were checked for extent of cell migration and HNK-1 expression in migratory cells. The results revealed that *BRE* promoted NCC migration, as the area covered by

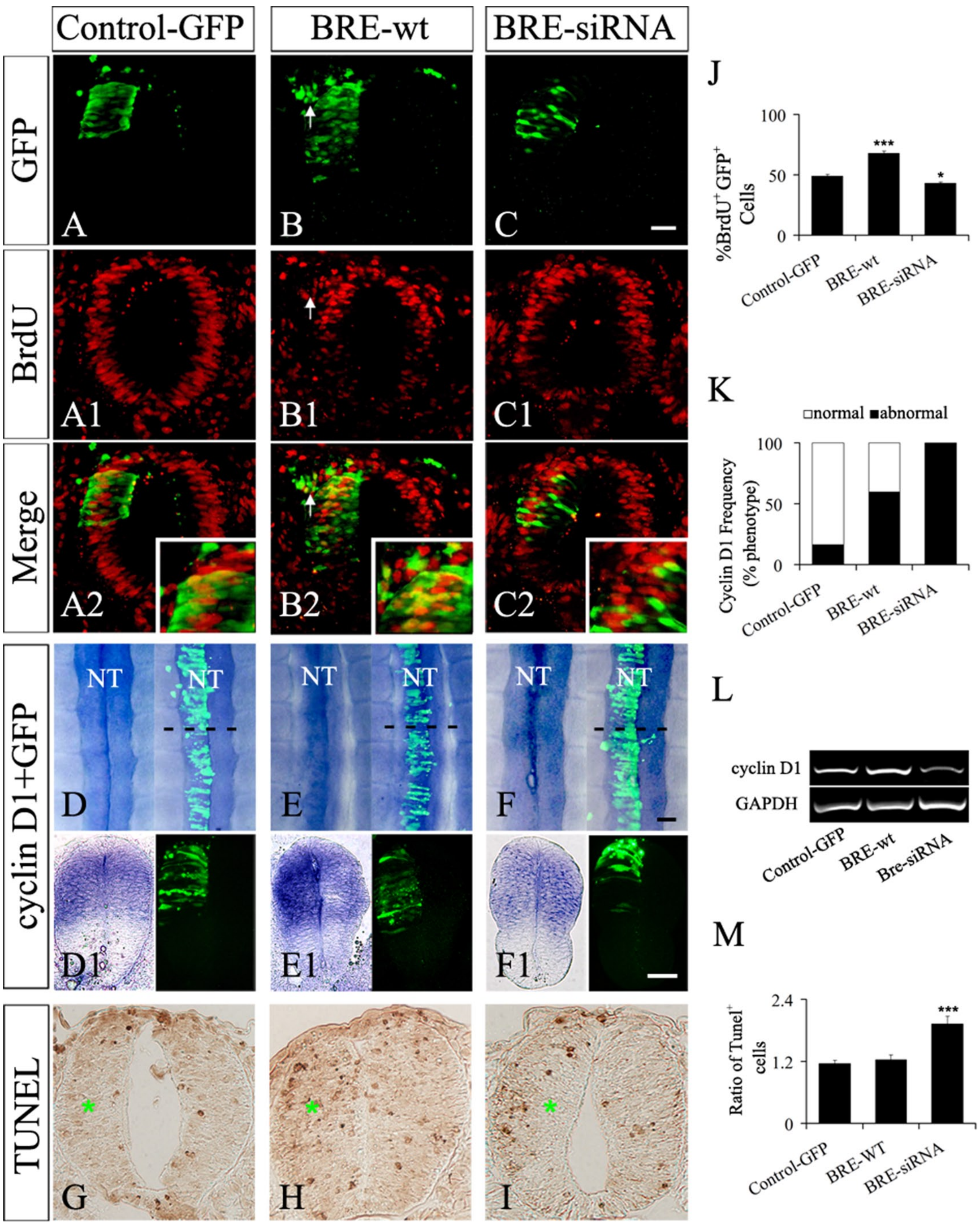

FIGURE 6: Ability of *BRE* to modulate cell cycle progression and survival in the developing neural tube. The neural tubes were unilaterally transfected with control-GFP (A), *BRE*-wt plus GFP (B), or *BRE*-siRNA plus GFP (C) constructs. (A1–C1) Transverse sections of the neural tube immunofluorescently stained for BrdU after transfection. (A2–C2) Merge images of BrdU incorporation and GFP marker expression. There are significantly more $BrdU^+/GFP^+$ cells in the *BRE*-wt–overexpressed samples (B2) than in the control-GFP samples (A2). Cyclin D1 expression after unilateral transfection of the neural tube (left side) with control-GFP (D), *BRE*-wt plus GFP (E), and *BRE*-siRNA plus GFP (F) constructs. In situ hybridization shows overexpressing *BRE* increased cyclin D1 expression (E, E1) as compared with the control (D, D1). Conversely, silencing *BRE* expression decreased cyclin D1 expression (F, F1). (G–I) TUNEL assay showing that overexpressing *BRE* did not increase apoptosis (H) compared with the control (G). However, silencing *BRE* increased the incidence of apoptosis (the transfected side of the neural tube is marked by a green asterisk). (J) Bar chart showing the ratio of $BrdU^+/GFP^+$ cells in neural tube transfected with control-GFP, *BRE*-wt, and *BRE*-siRNA constructs. $*p < 0.05$, $***p < 0.001$. (K) Bar chart displaying the incidence of normal and abnormal phenotypes resulting from *BRE* overexpression and silencing. Control-GFP ($N = 6$), *BRE*-wt ($N = 5$), and *BRE*-siRNA ($N = 6$) transfection. (L) Semiquantitative RT-PCR analysis showing that *BRE* overexpression in the neural tubes increased cyclin D1 expression, whereas silencing *BRE* reduced cyclin D1 expression ($N = 3$). (M) Bar chart showing that silencing *BRE* expression significantly increased apoptosis. Ratio of $TUNEL^+$ cells in the transfected side of the neural tube vs. the contralateral control side ($N = 6$, $***p < 0.001$). Error bars, SE. Scale bars, 20 μm (A–C, G–I, D1–F1), 100 μm (D–F). NT, neural tube.

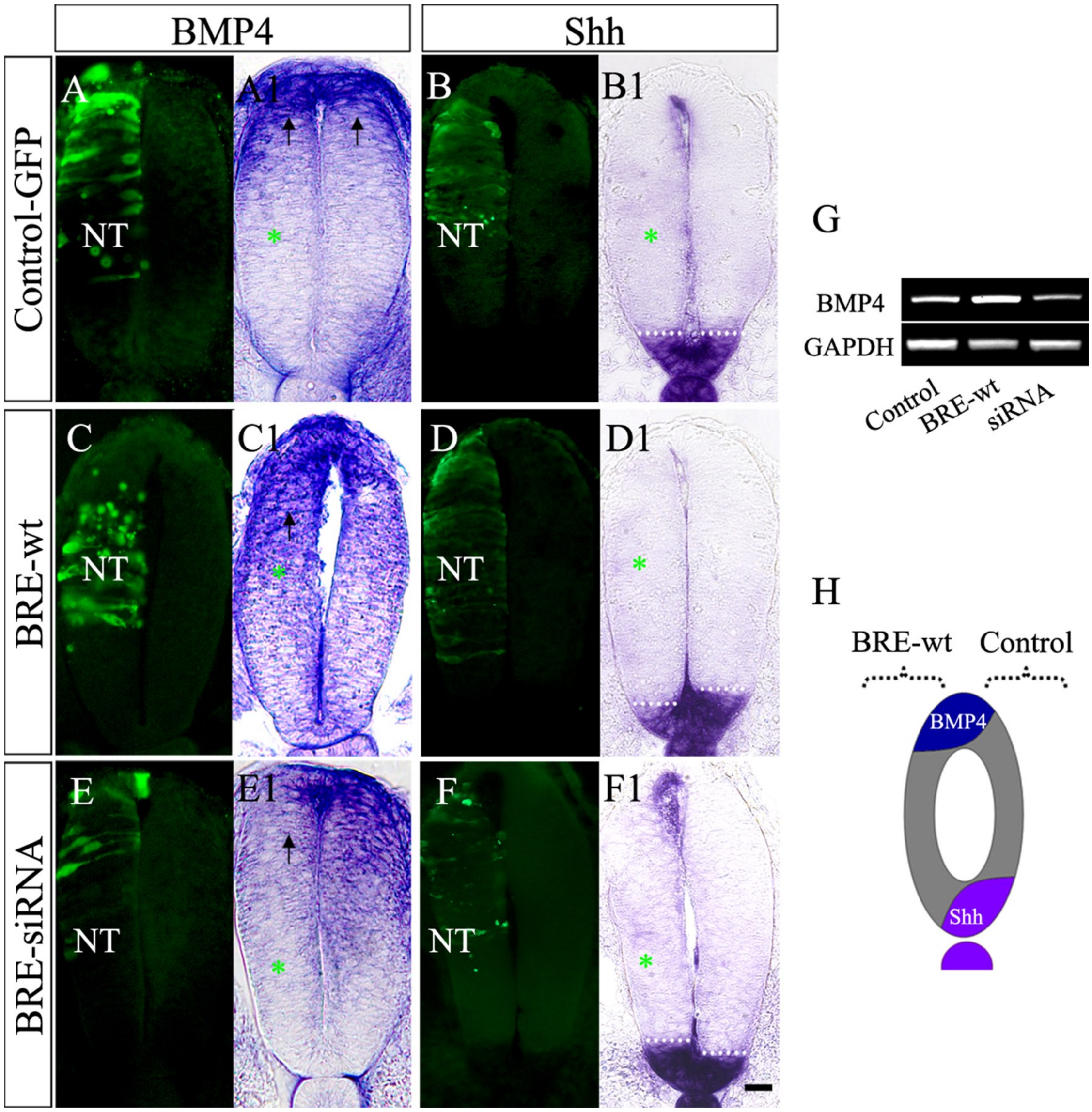

FIGURE 7: *BRE* affects BMP4 and Shh expression in the chick neural tube. HH10 neural tubes were unilaterally (green asterisks) transfected with control-GFP (A, B), *BRE*-wt plus GFP (C, D), and *BRE*-siRNA plus GFP (E, F) constructs. After 20 h, in situ hybridization was performed to establish BMP4 and Shh expression. (A1, B1) Normal expression pattern for BMP4 (black arrows in A1) and Shh on both sides of the neural tube. Shh expression is symmetrically distributed in the neural tube, as indicated by the dotted white line in B1. (C1, D1) *BRE* overexpression enhanced BMP4 expression (black arrows) in the dorsal neural tube compared with the untransfected side. In contrast, Shh expression was reduced in the *BRE*-overexpressed side of the neural tube, as indicated by the dotted white line in D1. (E1, F1) Silencing *BRE* represses BMP4 expression (black arrow in E1) compared with the contralateral, untransfected side of the neural tube. In contrast, Shh expression slightly increased compared to the untransfected side (dotted line in F1). (G) Neural tubes were collected for RT-PCR analysis after BE overexpression and silencing. Overexpressing *BRE* increased BMP4 expression, whereas silencing *BRE* suppressed BMP4, compared with the control ($N = 3$). (H) Schematic illustration showing *BRE* promoting BMP4 expression and suppressing Shh expression in the chick neural tube. Scale bar, 20 μm (A–F). NT, neural tube

migrating cells increased when *BRE* was up-regulated (1.85 ± 0.28 mm^2, $N = 5$, $p < 0.01$). In contrast, when *BRE* was down-regulated, the area covered by migrating cells was significantly reduced (0.56 ± 0.19 mm^2, $N = 4$, $p < 0.05$) when compared with control GFP explants (1.09 ± 0.17 mm^2, $N = 4$; Figure 8, C–F and K). In addition, there were significantly more HNK-1$^+$ cells in the *BRE*-overexpressing explants (78.88 ± 5.22%; $p < 0.001$) and significantly fewer HNK-1$^+$ cells in the *BRE*-silenced explants (31.88 ± 5.05%; $p < 0.01$) compared with the control explants (39.75 ± 3.45%, Figure 8, G–J1 and L). However, NCC migration of the *BRE*-wt–transfected tube was significantly inhibited in the LDN-193189 culture group (area, 0.81 ± 0.44 mm^2; HNK-1$^+$ cell percentage, 44.16 ± 5.16%) compared with the *BRE*-wt–transfected tube in control culture ($p < 0.001$).

DISCUSSION

We recently reported that *BRE* is important for maintaining stemness in human umbilical cord perivascular mesenchymal stem cells. We found that silencing *BRE* expression in these cells could dramatically accelerate osteogenic induction and differentiation (Chen *et al.*, 2013). This observation suggests that *BRE* may potentially play a role in development, but the function of this gene

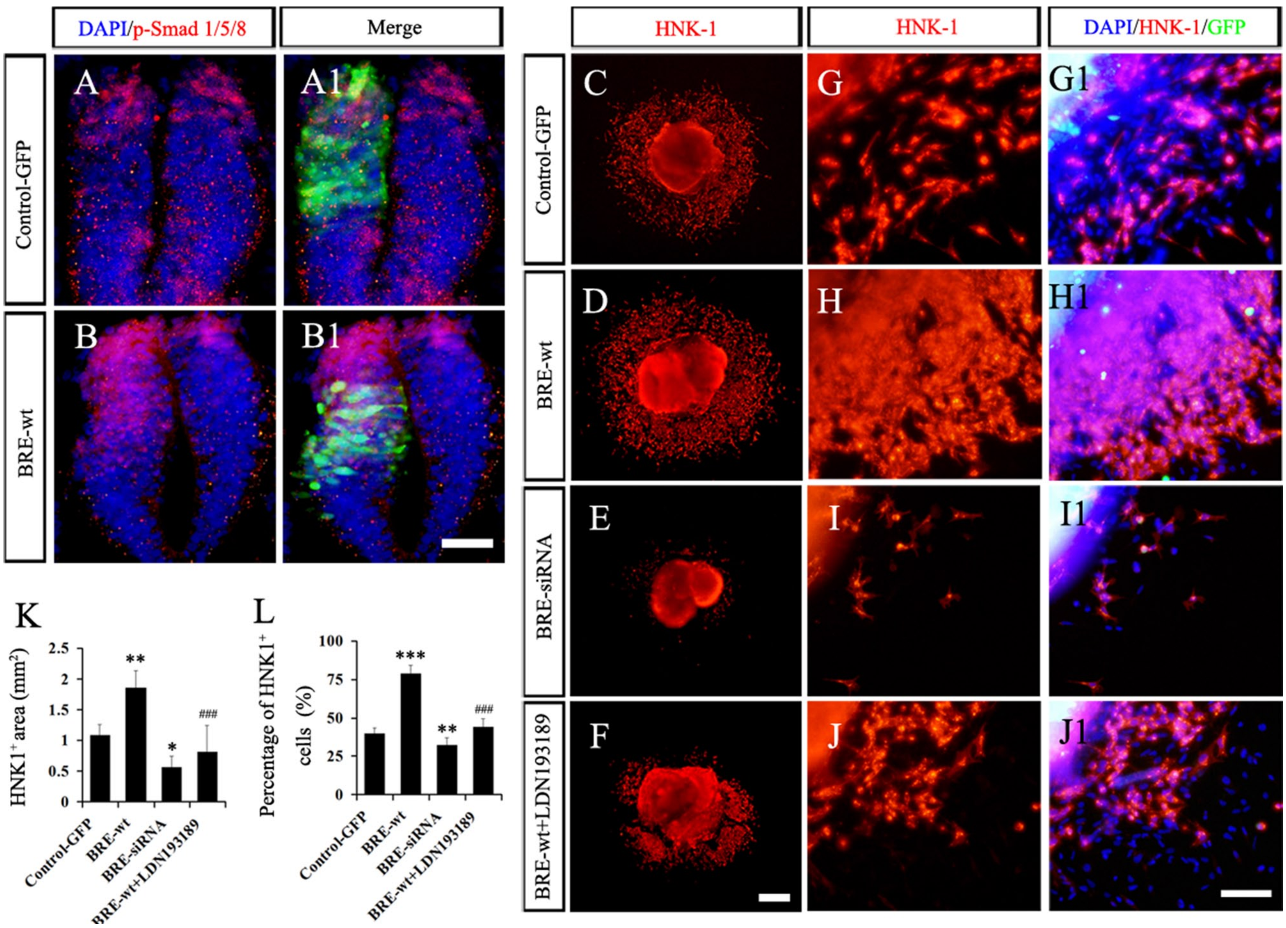

FIGURE 8: *BRE* modulates NCC migration through activation of BMP signaling. (A, A1) Transverse sections of neural tube immunofluorescently stained for p-Smad1/5/8 after transfection of the control-GFP. (B, B1Transverse sections of neural tube immunofluorescently stained for p-Smad1/5/8 after transfection of the *BRE*-wt. (C–F) Cultured neural tube explants transfected with control-GFP + control-siRNA (C), *BRE*-wt (D), control-GFP + *BRE*-siRNA (E), or *BRE*-wt with LDN-193189 added (F), immunofluorescently stained for HNK-1. (G–J) Higher-magnification images of C–F (top left corner shows the edge of the neural tube). (G1–J1) Merged images (DAPI, HNK-1, and GFP). (K) Area occupied by HNK$^+$ migratory cells. Image-Pro Plus 6.0 software was used to analyze the data. (L) Ratio of HNK-1$^+$ to total number of cells in each sample. *$p < 0.05$, **$p < 0.01$, and ***$p < 0.001$ indicate significant difference between experimental and control-GFP groups. $^{###}p < 0.001$ indicates significant difference between *BRE*-wt and *BRE*-wt+LDN-193189 embryos. Scale bars, 50 μm (A–B1), 500 μm (C–F), 100 μm (G–J1). Error bars, SD.

in embryogenesis had never been investigated. The early chick embryo is a good model for determining the multifunctional nature of the *BRE* gene during development. In adult mice, *BRE* is mainly expressed in the nervous system and its precursors (Li *et al*., 1995; Miao *et al*., 2001), and consistent with this, we found *BRE* expressed in the neural plate of primitive streak–stage embryos and in the neural tube of older embryos. We also detected *BRE* expression in the cranial NCCs. In this context, we decided to manipulate *BRE* gene expression in the neural tube of all experiments since the tissue normally express high levels of *BRE* during early embryonic development. Of interest, either overexpression or knockdown of *BRE* expression in the neural tube affected somites as the embryo developed. Our data suggest that this is due to the effect of *BRE* on expression of morphogenes involved in dorsoventral neural tube patterning and on NCCs.

In ovo electroporation, a widely used method in the chick embryo (Itasaki *et al*., 1999), allowed us to transfect half of the neural tube with *BRE* constructs while the contralateral half was left untransfected and served as control. Surprisingly, we found that overexpressing and silencing *BRE* in the chick neural tube did affect neural tube patterning genes BMP4 and Shh but affected the morphology of the flanking somites. When *BRE* was overexpressed, we found that the somites opposing the side that overexpressed *BRE* were significantly larger than those on the control side. The inverse effect was elicited when *BRE* expression in the neural tube was silenced. Because Pax7 is expressed in dorsal neural tube and upper-lateral somites (Otto *et al*., 2006; Galli *et al*., 2008), it was used to mark the process of somite differentiation after transfection of *BRE* in the neural tube (Figure 2). This suggests that misexpression of *BRE* in the neural tube can indirectly affect somitogenesis. It is now well established that the neural tube, somites, and notochord all interact intimately to regulate each other's development (Patten and Placzek, 2002; Ulloa and Marti, 2010).

The NCCs normally delaminate from the region between the dorsal neural tube and overlying ectoderm and migrate out toward the periphery of the embryo. Therefore we investigated whether these cells were directly affected when *BRE* was misexpressed in the neural tube. We used HNK-1 as the marker for migrating NCCs (Tucker *et al*., 1984) and found that overexpressing *BRE* increased HNK-1$^+$ NCC emigration. It was reported that transcription factor FoxD3 induced NCC delamination, and Sox9 was down-regulated after NCCs initiated their migration

(McKeown *et al.*, 2005). This is consistent with our result that overexpressing *BRE* accelerates NCC migration. Sela-Donenfeld and Kalcheim (2000) proposed that the timing of NCC delamination was regulated by developing somites and that they serve as substrates for NCC migration. Because overexpressing *BRE* in the neural tube causes larger somites to develop, this may feed back to further enhance NCC migration.

The segmented peripheral nervous system in the trunk is generated by the ventral migration of NCCs, which invade the anterior sclerotome and then differentiate into metameric dorsal root and sympathetic ganglia (Kuo and Erickson, 2010). The ventral spinal motor axons also project through the somites in a segmental manner (Roffers-Agarwal and Gammill, 2009). We explored whether neurite outgrowth from the ventral neural tube was affected by *BRE* misexpression. We used NF and TuJ-1 as neuronal markers, since NF is an intermediate filament and TuJ-1 is a neuron-specific, class III β-tubulin. We found that overexpressing *BRE* enhanced neurite outgrowth, whereas silencing *BRE* inhibited outgrowth. It has been reported that the developing motor and sensory axons are intimately associated with their surrounding tissues, which help to direct and guide axon growth (Tannahill *et al.*, 1997). Motor axons turn or branch away after encountering the posterior sclerotome cells, whereas the anterior sclerotome stimulates axon motility (Oakley and Tosney, 1993). This suggests that neurite outgrowth across somites might also act as a medium between neural tube signaling and somite development.

For neural tube to develop normally, it relies on a correct balance between cell proliferation and apoptosis in the neuroepithelium (Wei *et al.*, 2012). Cell proliferation is an essential process found in every aspect of embryo development, especially during the early developmental stages (Fu *et al.*, 2006). This is why early embryos are susceptible to changes in the external microenvironment. We performed BrdU-incorporation assays and determined that overexpressing *BRE* accelerated NCCs and neuroepithelial cells into S phase, whereas silencing *BRE* inhibited this process. We also examined other cell cycle–related genes, such as cyclin D1 (Figure 6, D–F, and L), p53, and BRCA1 (Supplemental Figure S1, H and I), to further establish an association between *BRE* and cell cycle. We found that *BRE* regulated NCC migration and cell cycle by modulating transcription of cyclin D1, which is similar to what was previously reported: the cytoplasmic N-cadherin fragment translocates into the nucleus, stimulates cyclin D1 transcription and crest delamination, and enhances transcription of β-catenin (Shoval *et al.*, 2007). It was also reported that p53 can coordinate NCC growth and EMT delamination by altering the expression of cell cycle–related genes (Rinon *et al.*, 2011). We found that overexpressing *BRE* down-regulated p53 expression. The BRCA1 protein complex forms from an assembly of proteins, RAP80/CCDC98/BRCC36/*BRE*/MERIT40/BRCA1, at the site of DNA breakage and plays a pivotal role in DNA repair and maintenance of genomic integrity. Increased apoptosis is caused by BRCA1 depletion, and this involves the p53 pathway (Pulvers and Huttner, 2009). This suggests that the cell survival effects seen in the neuroepithelium after *BRE* transfection might be attributed to the disturbance of p53 pathway.

The neurites are initially formed as outgrowths from the anterior horns of the spinal cord, in which *BRE* might be involved in regulating the neurogenesis through promoting Neurogenin2 expression (Figure 5L). BMP4 also regulates Neurogenin2 expression (Ota and Ito, 2006). The neurite outgrowth process is associated with Shh and BMP4 signaling from the notochord and the dorsal neural tube, respectively. Hence we investigated the expression patterns of BMP4 and Shh in the neural tube after *BRE* misexpression. We found BMP4 expression was significantly increased in the dorsal neural tube when we overexpressed *BRE*. This may explain why when we overexpressed *BRE* in the neural tube, oversized somites were produced, and there also was increased NCC migration. In support, we observed the inverse effect when *BRE* expression was silenced in the neural tube. Because BMP4 antagonizes Shh, we found that silencing *BRE* correspondingly increased Shh expression in the ventral neural tube because BMP4 expression was reduced dorsally by *BRE* knockdown.

BMPs achieve their inductive effects both locally, via direct cell–cell communication, and over a long range, via BMP-binding proteins, which establish diffusible BMP gradients (Hegarty *et al.*, 2013). The concentration of active BMP proteins (which deceases ventrally from the roof plate) is crucial for the dorsal/ventral patterning (Liu and Niswander, 2005). The transcription factors Smad1/5/8 are the pivotal intracellular effectors of the BMP family of proteins (Hegarty *et al.*, 2013). The results of p-Smad1/5/8 suggested that BMP signaling was activated after *BRE* overexpression. In early neurogenesis, BMP-Smad could act upstream of Wnt-β-catenin (Muller *et al.*, 2005), and BMP-Smad cooperates with Wnt-β-catenin signaling to control the neurogenesis (Muller *et al.*, 2005), with BMP-Smad important in the specification of neural fates and Wnt-β-catenin signaling functioning in appropriate proliferation (Hegarty *et al.*, 2013). These results suggested that the *BRE* affected neuroepithelial cell proliferation, differentiation, apoptosis, and NCC migration though both BMP-Smad and Wnt-β-catenin signaling.

In summary, *BRE* is mainly expressed in neural tube, NCCs, somites, and neurites during early embryo development. We altered *BRE* expression specifically in the neural tube, since it is capable of determining the development of NCCs, somites, and neurites. We found that overexpressing *BRE* could simultaneously enhance BMP4 and also inhibit Shh expression, dorsoventrally, in the neural tube. This may explain how *BRE* was able to enhance directly NCC migration and neurite outgrowth and also indirectly somite development. We schematically illustrate the role of *BRE* during early embryogenesis in Figure 9.

MATERIALS AND METHODS

Chick embryos

Fertilized leghorn eggs were acquired from the Avian Farm of South China Agriculture University (Guangzhou, China). The eggs were incubated in a humidified incubator (Yiheng Instruments, Shanghai, China) set at 38°C and 70% humidity until the embryos reached the desired developmental stage.

Gene transfection of chick embryos

pEGFP-N3 vector was purchased from Clontech, and *BRE*-siRNA was purchased from Guangzhou Ribobio. Full-length human *BRE* (*BRE*-wt) cDNA was ligated into the pEGFP-N3 vector. The plasmid DNAs were prepared and concentrated to 2 μg/μl using a Tiangen DP107-02 kit. The following strategy was designed for transfecting the different constructs into different stages of chick embryos according to experimental requirements. For in ovo electroporation, plasmid DNA were microinjected into the lumen of the neural tube of HH10-stage chick embryos. The electroporation parameters used for archiving maximum transfection efficiency were as previously described (Yang *et al.*, 2002; Wang *et al.*, 2013). The transfected chick embryos were then incubated at 38°C with 70% humidity until the embryos reached the HH13 stage. Some of these embryos were exposed to BrdU (10 μg/ml; Sigma-Aldrich, St. Louis, MO) for 2 h in Early Chick (EC) culture to determine the cell rate in S phase (Chapman *et al.*, 2001). The somatic level from the eighth to 13th pairs of somites (rostral to caudal) was used for analysis.

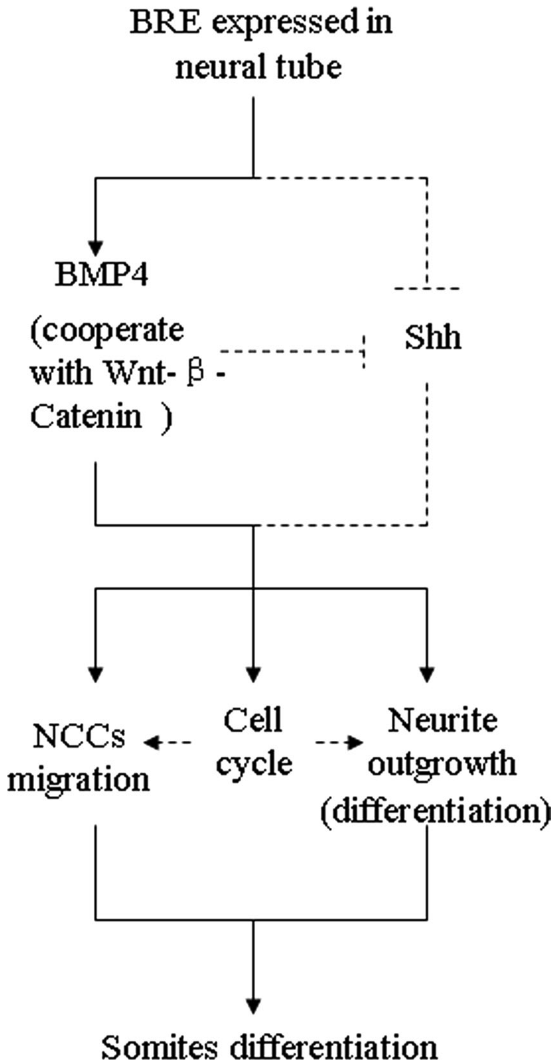

FIGURE 9: Model depicting how *BRE* misexpression in the neural tube can modulate somite development. Overexpression of *BRE* enhances BMP4 and inhibits Shh expression (possibly indirectly) in the neural tube. This would in turn affect the cell cycle through the activation of cell cycle–related genes. NCC migration and neurite outgrowth (neuron differentiation) are directly or indirectly enhanced by BMP4, Shh, and cell cycle. Finally, the enhanced NCC migration and neurite outgrowth might promote somite development.

Immunohistochemistry

Immunohistological staining was performed on whole-mount chick embryos to determine Pax7, HNK-1, TuJ-1, phospho-Smad1/5/8 (p-Smad1/5/8), β-catenin, and NF expression, as previously described (Yang *et al.*, 2008; Yue *et al.*, 2008). All embryos were fixed in 4% paraformaldehyde (PFA) at 4°C overnight and then washed with phosphate-buffered saline (PBS). The embryos were then blocked with 2% bovine serum albumin plus 1% Triton-X plus 1% Tween 20 in PBS for 2 h at room temperature to prevent unspecific immunoreaction. After several washes in PBS, the embryos were incubated with primary monoclonal antibody specific for Pax7 (1:100; Developmental Studies Hybridoma Bank, Iowa City, IA), HNK-1 (1:200; Sigma-Aldrich), TuJ-1 (1:200; Neuromics, Edina, MN), GFP (1:1000; Novus Biologicals, Littleton, CO), p-Smad1/5/8 (1:100, Cell Signaling, Boston, MA), β-catenin (1:100, Epitomics, Burlingame, CA), and NF (1:200; Invitrogen, Carlsbad, CA) overnight at 4°C on a rocker. After extensive washing, the embryos were incubated with anti-mouse or anti-rabbit Alexa Fluor 555 antibody (2 μg/ml; Invitrogen) overnight at 4°C on a rocker to reveal the primary antibody staining. Some embryos were pretreated with BrdU (10 μg/ml; Sigma-Aldrich) for 2 h and then immunohistological staining with BrdU antibody (1:200; BD Biosciences, San Jose, CA). All embryos were counterstained with 4′,6-diamidino-2-phenylindole (DAPI; 5 μg/ml; Invitrogen) for 1 h at room temperature. Subsequently the embryos were sectioned on a cryostat microtome (CM1900; Solms, Germany). The sections were mounted onto glass slides using Mowiol 4-88 mounting solution (Sigma-Aldrich) and sealed with coverslips.

In situ hybridization

BRE antisense probes were synthesized from a 1.2-kb *BRE* fragment inserted into a pGEMT vector. The *BRE*-pGEMT plasmid was cut with *Xho*1 and linearized to generate digoxigenin-labeled antisense *BRE* probes using T6 polymerase (Boehringer Mannheim Biochemica). Antisense probes that are specific for cyclin D1 (Shoval *et al.*, 2007), FGF8 (Yang *et al.*, 2002), BMP4 (Somi *et al.*, 2004), Snail2 (Nieto *et al.*, 1994), and Shh (Diez del Corral *et al.*, 2003) were also synthesized as previously described. Whole-mount in situ hybridization of chick embryos was performed according to a standard in situ hybridization protocol (Henrique *et al.*, 1995). Briefly the embryos were fixed with 4% PFA overnight at 4°C, dehydrated in a graded series of methanol, and stored at −20°C (overnight). The next day, the embryos were hybridized with *BRE* digoxigenin-labeled antisense probe overnight at 65°C. After hybridization, the bound RNA probe was visualized by incubation with alkaline phosphatase–conjugated anti-digoxigenin antibodies, and the color was developed in NBT/BCIP (Roche, Basel, Switzerland). The whole-mount stained embryos were photographed and then prepared for cryosectioning to a thickness of 15–20 μm on a cryostat microtome (Leica CM1900).

Analysis of programmed cell death

The extent of cell death in embryonic tissues was established by TUNEL analysis, using an *In Situ* Cell Death Detection Kit (Roche). The staining was performed according to the protocol provided by the manufacturer, which we adapted for whole-mount chick embryo labeling. TUNEL-positive cells were counted using Image Analysis Software (Olympus, Tokyo, Japan).

siRNA interference experiments

The *BRE*-siRNA corresponding to TCTGGCTGCACATCATTGA was custom designed to specifically target *BRE* mRNA; Ctrl-siRNA sequence was AAGCCUCGAAAUAUCUCCU (Tang *et al.*, 2006; Chen *et al.*, 2008). Both were purchased from Guangzhou Ribobio. The siRNA was diluted to a concentration of 1 mM in 20 mM KCl, 6 mM 4-(2-hydroxyethyl)-1-piperazineethanesulfonic acid (pH 7.5), and 200 mM $MgCl_2$. To track the siRNA transfection, we cotransfected *BRE*-siRNA or Ctrl-siRNA along with a pEGFP-N3 marker (1:1) in the half-side neural tube of HH10 chick embryos. The electroporation was performed using the same condition as described earlier.

RNA isolation, semiquantitative RT-PCR, and quantitative PCR

Transfected chick embryos (control-GFP, *BRE*-wt, and *BRE*-siRNA; *N* = 10 embryos for each group) were incubated at 38°C with 70% humidity until the embryos reached the HH13 stage. Total RNA was then isolated from the embryonic neural tube and somites using TRIzol (Invitrogen) according to the manufacturer's instructions. First-strand cDNA was synthesized at a final volume of 25 μl using a SuperScript III First-Strand kit (Invitrogen). After reverse transcription, RT-PCR amplification of the cDNA was performed using specific primers for chick *BRE* (5′-GCAGCCTTCCTGAGTCACTT-3′ and 5′-TGCTCTCTTGGCCATTTCGT-3′), Neurogenin2 (5′-TCTCCGTGATTTACGAGCGG-3′ and 5′-CGCTGTAATGTCCCGTGTCT-3′), β-catenin (5′-AGTTCTGGGAGCACAGCAAG-3′ and 5′-TGAACCATAACCGCAGCCTT-3′), Pax7 (5′-GCTTACTGAAGAGGTCCGACTGTG-3′ and 5′-ACAAGTTGATGCGAGGTGGAAGG-3′), cyclin D1 (5′-TCGGTGTCCTACTTCAAGTG-3′ and 5′ -GGAGTTGTCGGTGTAAATGC-3′), chick BMP4 (5′-AGGAGTGGCAGAAGTAG-3′ and 5′-CGGCTAATCCTGACGTGTTT-3′), and chick glyceraldehyde-3-phosphate dehydrogenase (5′-GTCAACGGATTTGGCCGTAT-3′ and 5′-AATGCCAAAGTTGTCATGGATG-3′) as previously described (Huber *et al.*, 2008; Endo *et al.*, 2012; Scott-Drechsel *et al.*, 2013). PCR was performed in a Bio-Rad S1000 thermal cycler (Bio-Rad, Hercules, CA). cDNAs were amplified for 30 cycles. One round of amplification was performed at 98°C for 10 s, at 60°C for 15 s, and at 72°C for 30 s (Takara, Japan). The PCR products (20 μl) were resolved on 1% agarose gels (Biowest, Spain) in 1× TAE buffer (0.04 M Tris-acetate and 0.001 M EDTA) and GeneGreen Nucleic Acid Dye (Tiangen, Beijing, China). The reaction products were visualized using a transilluminator (Syngene, Cambridge, United Kingdom) and a computer-assisted gel documentation system (Syngene). Quantitative PCR was also performed using SYBR Premix Ex Tag (Takara, Dalian, China) using a 7900HT Fast Real-Time PCR system (Applied Biosystems, Foster City, CA). The sets of primers used for quantitative PCR are provided in Supplemental Figure S6. Each of these experiments was replicated at least three times.

Primary explant culture

The neural tubes either alone or in the presence of somites of chick embryos (at stage HH10) were incubated in DMEM-F12 culture medium (Gibco, Grand Island, NY) or 200 nM LDN-193189 (SML0559; Sigma-Aldrich) DMEM-F12 inside an incubator (Galaxy S; RS Biotech, Scotland, UK) at 37°C and 5% CO_2 for 48 h. For analyzing the neural crest cell migration in vitro, the neural tubes cotransfected with *BRE*-siRNA, Ctrl-siRNA along with pEGFP-N3, or *BRE*-wt-GFP were excised from the embryos at the 1st–10th somite levels and then incubated in DMEM-F12 culture medium for the required time. The cultured explants were used for photography and immunofluorescence staining.

Photography

After immunohistological staining, the whole-mount embryos were photographed using a fluorescence stereomicroscope (MVX10; Olympus, Osaka, Japan) and imaging software (Image-Pro Plus 7.0). Sections of the stained embryos were photographed using an epifluorescence microscope (Olympus IX51, Leica DM 4000B) at 200× or 400× magnification using the Olympus software package (Leica CW4000 FISH).

Image acquisition and analysis

For the quantification in the BrdU experiments, we manually counted $BrdU^+$ GFP^+ cells versus $BrdU^+$ cells of the neural tube in the transfected side (Cayuso *et al.*, 2006); the HNK-1^+ area was quantified with Image-Pro Plus 6.0; for the primary explant culture experiments, cell migration was quantified by measuring HNK-1^+ staining with Image-Pro Plus 6.0; HNK-1^+ cells were manually counted on DAPI and HNK-1 merged images. The data are presented as mean ± SE or mean ± SD. Statistical analysis for the experimental data were performed using a SPSS 13.0 statistical package program for Windows. Statistical significance was established using one-way analysis of variance. $p < 0.05$ was considered to be significantly different.

ACKNOWLEDGMENTS

We thank Zheng-lai Ma, Jiang-chao Li, En-ni Chen, Chang Liang, and Shi-yao Zhang for technical help; Maurice van den Hoff for the BMP4 plasmid; Chaya Kalcheim for the cyclin D1 plasmid; and Qing Chang for invaluable input on the design of the experiments. This study was supported by NSFC grants (31401230; 31071054; 30971493); a Hong Kong General Research Fund Grant (469313); the China Postdoctoral Science Foundation (2014M560694); the Fundamental Research Funds for the Central Universities (21614319); and the Collaborated grant for HK-Macao-TW of the Ministry of Science and Technology (2012DFH30060).

REFERENCES

Agarwal ML, Agarwal A, Taylor WR, Stark GR (1995). p53 controls both the G2/M and the G1 cell cycle checkpoints and mediates reversible growth arrest in human fibroblasts. Proc Natl Acad Sci USA 92, 8493–8497.

Anderson C, Thorsteinsdottir S, Borycki AG (2009). Sonic hedgehog-dependent synthesis of laminin alpha1 controls basement membrane assembly in the myotome. Development 136, 3495–3504.

Becker EB, Bonni A (2005). Beyond proliferation—cell cycle control of neuronal survival and differentiation in the developing mammalian brain. Semin Cell Dev Biol 16, 439–448.

Bronner ME (2012). A career at the interface of cell and developmental biology: a view from the crest. Mol Biol Cell 23, 4151–4153.

Bronner ME, LeDouarin NM (2013). Development and evolution of the neural crest: an overview. Dev Biol 366, 2–9.

Cayuso J, Ulloa F, Cox B, Briscoe J, Marti E (2006). The Sonic hedgehog pathway independently controls the patterning, proliferation and survival of neuroepithelial cells by regulating Gli activity. Development 133, 517–528.

Chapman SC, Collignon J, Schoenwolf GC, Lumsden A (2001). Improved method for chick whole-embryo culture using a filter paper carrier. Dev Dyn 220, 284–289.

Chen E, Tang MK, Yao Y, Yau WW, Lo LM, Yang X, Chui YL, Chan J, Lee KK (2013). Silencing BRE expression in human umbilical cord perivascular (HUCPV) progenitor cells accelerates osteogenic and chondrogenic differentiation. PLoS One 8, e67896.

Chen HB, Pan K, Tang MK, Chui YL, Chen L, Su ZJ, Shen ZY, Li EM, Xie W, Lee KK (2008). Comparative proteomic analysis reveals differentially expressed proteins regulated by a potential tumor promoter, BRE, in human esophageal carcinoma cells. Biochem Cell Biol 86, 302–311.

Chiang C, Litingtung Y, Lee E, Young KE, Corden JL, Westphal H, Beachy PA (1996). Cyclopia and defective axial patterning in mice lacking Sonic hedgehog gene function. Nature 383, 407–413.

Ching AK, Li PS, Li Q, Chan BC, Chan JY, Lim PL, Pang JC, Chui YL (2001). Expression of human BRE in multiple isoforms. Biochem Biophys Res Commun 288, 535–545.

Christ B, Brand-Saberi B, Grim M, Wilting J (1992). Local signalling in dermomyotomal cell type specification. Anat Embryol 186, 505–510.

Christ B, Ordahl CP (1995). Early stages of chick somite development. Anat Embryol 191, 381–396.

Deng CX (2006). BRCA1: cell cycle checkpoint, genetic instability, DNA damage response and cancer evolution. Nucleic Acids Res 34, 1416–1426.

Diez del Corral R, Olivera-Martinez I, Goriely A, Gale E, Maden M, Storey K (2003). Opposing FGF and retinoid pathways control ventral neural pattern, neuronal differentiation, and segmentation during body axis extension. Neuron 40, 65–79.

Eckalbar WL, Fisher RE, Rawls A, Kusumi K (2013). Scoliosis and segmentation defects of the vertebrae. Wiley Interdiscip Rev Dev Biol 1, 401–423.

Endo Y, Ishiwata-Endo H, Yamada KM (2012). Extracellular matrix protein anosmin promotes neural crest formation and regulates FGF, BMP, WNT activities. Dev Cell 23, 305–316.

Francetic T, Li Q (2011). Skeletal myogenesis and Myf5 activation. Transcription 2, 109–114.

Fu J, Tay SS, Ling EA, Dheen ST (2006). High glucose alters the expression of genes involved in proliferation and cell-fate specification of embryonic neural stem cells. Diabetologia 49, 1027–1038.

Galli LM, Knight SR, Barnes TL, Doak AK, Kadzik RS, Burrus LW (2008). Identification and characterization of subpopulations of Pax3 and Pax7 expressing cells in developing chick somites and limb buds. Dev Dyn 237, 1862–1874.

Gu C, Castellino A, Chan JY, Chao MV (1998). BRE: a modulator of TNF-alpha action. FASEB J 12, 1101–1108.

Hegarty SV, O'Keeffe GW, Sullivan AM (2013). BMP-Smad 1/5/8 signalling in the development of the nervous system. Prog Neurobiol 109, 28–41.

Henrique D, Adam J, Myat A, Chitnis A, Lewis J, Ish-Horowicz D (1995). Expression of a Delta homologue in prospective neurons in the chick. Nature 375, 787–790.

Huang X, Saint-Jeannet JP (2004). Induction of the neural crest and the opportunities of life on the edge. Dev Biol 275, 1–11.

Huber K, Franke A, Bruhl B, Krispin S, Ernsberger U, Schober A, von Bohlen und Halbach O, Rohrer H, Kalcheim C, Unsicker K (2008). Persistent expression of BMP-4 in embryonic chick adrenal cortical cells and its role in chromaffin cell development. Neural Dev 3, 28.

Itasaki N, Bel-Vialar S, Krumlauf R (1999). "Shocking" developments in chick embryology: electroporation and in ovo gene expression. Nat Cell Biol 1, E203–E207.

Kageyama R, Niwa Y, Isomura A, Gonzalez A, Harima Y (2012). Oscillatory gene expression and somitogenesis. Wiley Interdiscip Rev Dev Biol 1, 629–641.

Kalcheim C (2011). Regulation of trunk myogenesis by the neural crest: a new facet of neural crest-somite interactions. Dev Cell 21, 187–188.

Koblar SA, Krull CE, Pasquale EB, McLennan R, Peale FD, Cerretti DP, Bothwell M (2000). Spinal motor axons and neural crest cells use different molecular guides for segmental migration through the rostral half-somite. J Neurobiol 42, 437–447.

Kranenburg O, van der Eb AJ, Zantema A (1996). Cyclin D1 is an essential mediator of apoptotic neuronal cell death. EMBO J 15, 46–54.

Kuo BR, Erickson CA (2010). Regional differences in neural crest morphogenesis. Cell Adh Migr 4, 567–585.

Lee KK, Webb SE, Cai DQ, Sze LY, Lam KH, Li Z, Paulin D (1995). Desmin transgene expression in mouse somites requires the presence of the neural tube. Int J Dev Biol 39, 469–475.

Li L, Yoo H, Becker FF, Ali-Osman F, Chan JY (1995). Identification of a brain- and reproductive-organs-specific gene responsive to DNA damage and retinoic acid. Biochem Biophys Res Commun 206, 764–774.

Liu A, Niswander LA (2005). Bone morphogenetic protein signalling and vertebrate nervous system development. Nat Rev Neurosci 6, 945–954.

Marcelle C, Stark MR, Bronner-Fraser M (1997). Coordinate actions of BMPs, Wnts, Shh and noggin mediate patterning of the dorsal somite. Development 124, 3955–3963.

McKeown SJ, Lee VM, Bronner-Fraser M, Newgreen DF, Farlie PG (2005). Sox10 overexpression induces neural crest-like cells from all dorsoventral levels of the neural tube but inhibits differentiation. Dev Dyn 233, 430–444.

Miao J, Panesar NS, Chan KT, Lai FM, Xia N, Wang Y, Johnson PJ, Chan JY (2001). Differential expression of a stress-modulating gene, BRE, in the adrenal gland, in adrenal neoplasia, and in abnormal adrenal tissues. J Histochem Cytochem 49, 491–500.

Muller T, Anlag K, Wildner H, Britsch S, Treier M, Birchmeier C (2005). The bHLH factor Olig3 coordinates the specification of dorsal neurons in the spinal cord. Genes Dev 19, 733–743.

Munsterberg AE, Kitajewski J, Bumcrot DA, McMahon AP, Lassar AB (1995). Combinatorial signaling by Sonic hedgehog and Wnt family members induces myogenic bHLH gene expression in the somite. Genes Dev 9, 2911–2922.

Murtaugh LC, Chyung JH, Lassar AB (1999). Sonic hedgehog promotes somitic chondrogenesis by altering the cellular response to BMP signaling. Genes Dev 13, 225–237.

Nieto MA, Sargent MG, Wilkinson DG, Cooke J (1994). Control of cell behavior during vertebrate development by Slug, a zinc finger gene. Science 264, 835–839.

Noden DM, Marcucio R, Borycki AG, Emerson CPJr (1999). Differentiation of avian craniofacial muscles: I. Patterns of early regulatory gene expression and myosin heavy chain synthesis. Dev Dyn 216, 96–112.

Oakley RA, Tosney KW (1993). Contact-mediated mechanisms of motor axon segmentation. J Neurosci 13, 3773–3792.

Ota M, Ito K (2006). BMP and FGF-2 regulate neurogenin-2 expression and the differentiation of sensory neurons and glia. Dev Dyn 235, 646–655.

Otto A, Schmidt C, Patel K (2006). Pax3 and Pax7 expression and regulation in the avian embryo. Anat Embryol 211, 293–310.

Patten I, Placzek M (2002). Opponent activities of Shh and BMP signaling during floor plate induction in vivo. Curr Biol 12, 47–52.

Pulvers JN, Huttner WB (2009). Brca1 is required for embryonic development of the mouse cerebral cortex to normal size by preventing apoptosis of early neural progenitors. Development 136, 1859–1868.

Resende TP, Ferreira M, Teillet MA, Tavares AT, Andrade RP, Palmeirim I (2010). Sonic hedgehog in temporal control of somite formation. Proc Natl Acad Sci USA 107, 12907–12912.

Ribes V, Briscoe J (2009). Establishing and interpreting graded Sonic Hedgehog signaling during vertebrate neural tube patterning: the role of negative feedback. Cold Spring Harb Perspect Biol 1, a002014.

Rinon A, Molchadsky A, Nathan E, Yovel G, Rotter V, Sarig R, Tzahor E (2011). p53 coordinates cranial neural crest cell growth and epithelial-mesenchymal transition/delamination processes. Development 138, 1827–1838.

Rios AC, Serralbo O, Salgado D, Marcelle C (2011). Neural crest regulates myogenesis through the transient activation of NOTCH. Nature 473, 532–535.

Roffers-Agarwal J, Gammill LS (2009). Neuropilin receptors guide distinct phases of sensory and motor neuronal segmentation. Development 136, 1879–1888.

Scott-Drechsel DE, Rugonyi S, Marks DL, Thornburg KL, Hinds MT (2013). Hyperglycemia slows embryonic growth and suppresses cell cycle via cyclin D1 and p21. Diabetes 62, 234–242.

Sela-Donenfeld D, Kalcheim C (2000). Inhibition of noggin expression in the dorsal neural tube by somitogenesis: a mechanism for coordinating the timing of neural crest emigration. Development 127, 4845–4854.

Sela-Donenfeld D, Kalcheim C (2002). Localized BMP4-noggin interactions generate the dynamic patterning of noggin expression in somites. Dev Biol 246, 311–328.

Serralbo O, Marcelle C (2014). Migrating cells mediate long-range WNT signaling. Development 141, 2057–2063.

Shoval I, Ludwig A, Kalcheim C (2007). Antagonistic roles of full-length N-cadherin and its soluble BMP cleavage product in neural crest delamination. Development 134, 491–501.

Simmons AD, Horton S, Abney AL, Johnson JE (2001). Neurogenin2 expression in ventral and dorsal spinal neural tube progenitor cells is regulated by distinct enhancers. Dev Biol 229, 327–339.

Somi S, Buffing AA, Moorman AF, Van Den Hoff MJ (2004). Dynamic patterns of expression of BMP isoforms 2, 4, 5, 6, 7 during chicken heart development. Anat Rec 279, 636–651.

Tang MK, Wang CM, Shan SW, Chui YL, Ching AK, Chow PH, Grotewold L, Chan JY, Lee KK (2006). Comparative proteomic analysis reveals a function of the novel death receptor-associated protein BRE in the regulation of prohibitin and p53 expression and proliferation. Proteomics 6, 2376–2385.

Tannahill D, Cook GM, Keynes RJ (1997). Axon guidance and somites. Cell Tissue Res 290, 275–283.

Tucker GC, Aoyama H, Lipinski M, Tursz T, Thiery JP (1984). Identical reactivity of monoclonal antibodies HNK-1 and NC-1: conservation in vertebrates on cells derived from the neural primordium and on some leukocytes. Cell Differ 14, 223–230.

Ulloa F, Marti E (2010). Wnt won the war: antagonistic role of Wnt over Shh controls dorso-ventral patterning of the vertebrate neural tube. Dev Dyn 239, 69–76.

Van Ho AT, Hayashi S, Brohl D, Aurade F, Rattenbach R, Relaix F (2011). Neural crest cell lineage restricts skeletal muscle progenitor cell differentiation through Neuregulin1-ErbB3 signaling. Dev Cell 21, 273–287.

Wang G, Li Y, Wang XY, Han Z, Chuai M, Wang LJ, Ho Lee KK, Geng JG, Yang X (2013). Slit/Robo1 signaling regulates neural tube development by balancing neuroepithelial cell proliferation and differentiation. Exp Cell Res 319, 1083–1093.

Wei X, Li H, Miao J, Zhou F, Liu B, Wu D, Li S, Wang L, Fan Y, Wang W, Yuan Z (2012). Disturbed apoptosis and cell proliferation in developing neuroepithelium of lumbo-sacral neural tubes in retinoic acid-induced spina bifida aperta in rat. Int J Dev Neurosci 30, 575–581.

Wilson L, Maden M (2005). The mechanisms of dorsoventral patterning in the vertebrate neural tube. Dev Biol 282, 1–13.

Yang X, Chrisman H, Weijer CJ (2008). PDGF signalling controls the migration of mesoderm cells during chick gastrulation by regulating N-cadherin expression. Development 135, 3521–3530.

Yang X, Dormann D, Munsterberg AE, Weijer CJ (2002). Cell movement patterns during gastrulation in the chick are controlled by positive and negative chemotaxis mediated by FGF4 and FGF8. Dev Cell 3, 425–437.

Yu PB, Deng DY, Lai CS, Hong CC, Cuny GD, Bouxsein ML, Hong DW, McManus PM, Katagiri T, Sachidanandan C, *et al.* (2008). BMP type I receptor inhibition reduces heterotopic [corrected] ossification. Nat Med 14, 1363–1369.

Yue Q, Wagstaff L, Yang X, Weijer C, Munsterberg A (2008). Wnt3a-mediated chemorepulsion controls movement patterns of cardiac progenitors and requires RhoA function. Development 135, 1029–1037.